J|A|C|S
ARTICLES
Published on Web 12/08/2006

Targeting of Cancer Cells with Ferrimagnetic Ferritin Cage Nanoparticles

Masaki Uchida,[†,‡] Michelle L. Flenniken,[‡,§] Mark Allen,[†,‡] Deborah A. Willits,[‡,||] Bridgid E. Crowley,[†,‡] Susan Brumfield,[‡,||] Ann F. Willis,[†,‡] Larissa Jackiw,[‡,⊥] Mark Jutila,[‡,⊥] Mark J. Young,*[,‡,||] and Trevor Douglas*[,†,‡]

Contribution from the Departments of Chemistry and Biochemistry, Microbiology, Plant Sciences, and Veterinary Molecular Biology and the Center for Bio-Inspired Nanomaterials (CBIN), Montana State University, Bozeman, Montana 59717

Received August 1, 2006; E-mail: tdouglas@chemistry.montana.edu; myoung@montana.edu

Abstract: Protein cage architectures such as virus capsids and ferritins are versatile nanoscale platforms amenable to both genetic and chemical modification. Incorporation of multiple functionalities within these nanometer-sized protein architectures demonstrate their potential to serve as functional nanomaterials with applications in medical imaging and therapy. In the present study, we synthesized an iron oxide (magnetite) nanoparticle within the interior cavity of a genetically engineered human H-chain ferritin (HFn). A cell-specific targeting peptide, RGD-4C which binds $\alpha_v\beta_3$ integrins upregulated on tumor vasculature, was genetically incorporated on the exterior surface of HFn. Both magnetite-containing and fluorescently labeled RGD4C-Fn cages bound C32 melanoma cells in vitro. Together these results demonstrate the capability of a genetically modified protein cage architecture to serve as a multifunctional nanoscale container for simultaneous iron oxide loading and cell-specific targeting.

Introduction

The intersection of chemistry, biology, and nanotechnology is expected to make significant contributions to the field of medical diagnosis and therapeutics. For example, quantum dots or fluorochrome-conjugated macromolecules have been developed for cell and tissue imaging agents.[1−4] Iron oxide nanoparticles are being developed for use in biomedical applications such as hyperthermia cancer therapy and as magnetic resonance imaging (MRI) contrast agents.[5−16]

The utility of iron oxide nanoparticles for biomedical applications is dependent on the size homogeneity, magnetic properties, and the ability to target specific cells and/or tissues. Preparation of nanoparticles of a desired size, with narrow size distribution, is critical because magnetic properties of iron oxide particle are significantly affected by particle size. The simultaneous incorporation of cell-specific targeting could allow precise imaging of desired tissues such as tumors. The aim of this study is to demonstrate that a single protein cage architecture possesses the chemical plasticity to both form ferromagnetic iron oxide nanoparticles with narrow size distribution and simultaneously incorporate an active cell-specific targeting ligand on the protein cage exterior.

Protein cage architectures are precisely assembled from a limited number of protein subunits and present three distinct interfaces that can be exploited in order to impart functionality by design: the interior, exterior, and the interface between subunits.[17,18] The subunits have versatility in that they can be easily modified using genetic and chemical means. We are therefore able to simultaneously impart multiple functionality (targeting and mineralization/entrapment) to a single protein cage.[3,19,20]

[†] Department of Chemistry and Biochemistry.
[‡] CBIN.
[§] Department of Microbiology.
[||] Department of Plant Sciences.
[⊥] Department of Veterinary Molecular Biology.

(1) Medintz, I. L.; Uyeda, H. T.; Goldman, E. R.; Mattoussi, H. *Nat. Mater.* **2005**, *4* (6), 435.
(2) Michalet, X.; Pinaud, F. F.; Bentolila, L. A.; Tsay, J. M.; Doose, S.; Li, J. J.; Sundaresan, G.; Wu, A. M.; Gambhir, S. S.; Weiss, S. *Science* **2005**, *307* (5709), 538.
(3) Flenniken, M. L.; Willits, D. A.; Harmsen, A. L.; Liepold, L. O.; Harmsen, A. G.; Young, M. J.; Douglas, T. *Chem. Biol.* **2006**, *13* (2), 161.
(4) Lewis, J. D.; Destito, G.; Zijlstra, A.; Gonzalez, M. J.; Quigley, J. P.; Manchester, M.; Stuhlmann, H. *Nat. Med.* **2006**, *12* (3), 354.
(5) Bulte, J. W. M.; Douglas, T.; Mann, S.; Frankel, R. B.; Moskowitz, B. M.; Brooks, R. A.; Baumgarner, C. D.; Vymazal, J.; Strub, M.-P.; Frank, J. A. *J. Magn. Reson. Imaging* **1994**, *4*, 497.
(6) Jung, C. W.; Jacobs, P. *Magn. Reson. Imaging* **1995**, *13* (5), 661.
(7) Shinkai, M.; Yanase, M.; Honda, H.; Wakabayashi, T.; Yoshida, J.; Kobayashi, T. *Jpn. J. Cancer Res.* **1996**, *87* (11), 1179.
(8) Bulte, J. W. M.; Douglas, T.; Witwer, B.; Zhang, S. C.; Strable, E.; Lewis, B. K.; Zywicke, H.; Miller, B.; van Gelderen, P.; Moskowitz, B. M.; Duncan, I. D.; Frank, J. A. *Nat. Biotechnol.* **2001**, *19* (12), 1141.
(9) Frank, J. A.; Miller, B. R.; Arbab, A. S.; Zywicke, H. A.; Jordan, E. K.; Lewis, B. K.; Bryant, L. H.; Bulte, J. W. M. *Radiology* **2003**, *228* (2), 480.
(10) Ito, A.; Kuga, Y.; Honda, H.; Kikkawa, H.; Horiuchi, A.; Watanabe, Y.; Kobayashi, T. *Cancer Lett.* **2004**, *212* (2), 167.
(11) Yancy, A. D.; Olzinski, A. R.; Hu, T. C. C.; Lenhard, S. C.; Aravindhan, K.; Gruver, S. M.; Jacobs, P. M.; Willette, R. N.; Jucker, B. M. *J. Magn. Reson. Imaging* **2005**, *21* (4), 432.
(12) Gupta, A. K.; Gupta, M. *Biomaterials* **2005**, *26* (18), 3995.
(13) Kawashita, M.; Tanaka, M.; Kokubo, T.; Inoue, Y.; Yao, T.; Hamada, S.; Shinjo, T. *Biomaterials* **2005**, *26* (15), 2231.
(14) Gupta, A. K.; Curtis, A. S. G. *J. Mater. Sci.: Mater. Med.* **2004**, *15* (4), 493.
(15) Song, H. T.; Choi, J. S.; Huh, Y. M.; Kim, S.; Jun, Y. W.; Suh, J. S.; Cheon, J. *J. Am. Chem. Soc.* **2005**, *127*, 9992.
(16) Lee, H.; Lee, E.; Kim, D. K.; Jang, N. K.; Jeong, Y. Y.; Jon, S. *J. Am. Chem. Soc.* **2006**, *128*, 7383.
(17) Douglas, T.; Young, M. *Science* **2006**, *312* (5775), 873.
(18) Uchida, M.; Klem, M. T.; Allen, M.; Suci, P.; Flenniken, M. L.; Gillitzer, E.; Varpness, Z.; Young, M.; Douglas, T. *Adv. Mater.*, in press.

10.1021/ja0655690 CCC: $33.50

The interior cavity of the protein architecture can act as a size-constrained reaction vessel for synthesis of nanoparticles with narrow size distribution.[17,18] The protein cage containers themselves have an extremely homogeneous size distribution, and this homogeneity of the template leads to homogeneity of the templated material. Various inorganic nanoparticles have been synthesized within a range of protein cage architectures.[21−37] Although the container-like protein cages share common features being comprised of a limited number of protein subunits to form container-like architectures, there is no single protein cage which perfectly satisfies the required chemical properties for all nanoparticle synthesis. To prepare ferrimagnetic iron oxide nanoparticles, ferritins are perhaps the best choice of protein cage due to their inherent native function which is the sequestration and storage of Fe as Fe_2O_3.[38−40]

Ferritins are a family of proteins found in all domains of life, which are composed of 24 subunits to form a cage architecture of 12 nm diameter with an interior cavity of 8 nm diameter.[41] Mammalian ferritins consist of a mixture of two different types of subunits known as H (heavy) and L (light) chain.[39] H chain includes a catalytic ferroxidase site, which catalyzes the oxidation of Fe(II) to Fe(III), but this site is absent from the L chain subunit.[41] In ferritin, oxidation of Fe(II) to Fe(III) leads to nucleation of iron oxide due to the insolubility of Fe(III). In this study, we show that a genetically engineered ferritin mutant, comprised of only H chain subunits, has distinct advantages as a nanoscale template for iron oxide nanoparticle synthesis.

Cell-targeting moieties can be exposed on the exterior surface of protein cage architectures by means of both genetic and chemical modification.[3,42] It has been shown by in vivo phage display techniques that certain small peptides are able to selectively target to the vasculature of a variety of tissues, organs, and tumors.[43−46] One representative example of this is the RGD-4C peptide (CDCRGDCFC), which binds selectively to integrins $\alpha_v\beta_3$ and $\alpha_v\beta_5$ which are up-regulated on rapidly dividing cells.[43] Since these integrins are up-regulated in angiogenic tumor vasculature, the RGD-4C peptide can be utilized as a cancer cell targeting ligand. It has been demonstrated that RGD-4C conjugated to a small heat shock protein (sHsp) or quantum dots, as well as RGD-4C conjugated to the anti-cancer agent, doxorubicin, all exhibit cancer cell targeting specificity.[3,47,48]

In the present work, we investigated the capacity of the ferritin to incorporate RGD-4C peptide on its exterior surface without disrupting the overall cage architecture or the ability of the protein to spatially direct the biomimetic mineralization to ferrimagnetic iron oxide nanoparticles. We also investigated the in vitro cancer cell specific targeting of the RGD-4C ferritin variant.

Experimental Section

Cloning of Human H Chain Ferritin (HFn). Human normal skeletal muscle cDNA was obtained from Invitrogen (D8090-01; Carlsbad, CA). The gene encoding the human H chain ferritin (HFn) was amplified by polymerase chain reaction (PCR) using a forward primer (5′ A GTC GCC **CAT ATG** ACG ACC GCG TCC 3′; boldfacing delineates an *Nde*I site) and reverse primer (5′ GCC **GGA TCC** TTA GCT TTC ATT ATC AC 3′; boldfacing delineates a *Bam*HI site) for amplification. The PCR 572 bp product was subsequently cloned into the *Nde*I and *Bam*HI restriction sites of the pET-30a(+) plasmid (Novagen). The plasmid vector was transformed into XL2 Blue ultracompetent *Escherichia coli* (*E. coli*; Stratagene, La Jolla, CA) and plated on LB with kanamycin plates for selection. Positive colonies were grown overnight in 3 mL of LB with 30 mg/L kanamycin medium. The HFn plasmid DNA was isolated using Perfectprep Plasmid Mini (Effendorf, Hamburg, Germany) and inserted DNA was sequenced on an ABI 310 automated capillary sequencer using Big Dye chain termination sequence technology (Applied Biosystem, Foster City, CA).

Mutagenesis of RGD-4C Peptide Conjugated Ferritin (RGD4C-Fn). The N-terminal of the HFn is exposed on the exterior surface of the assembled ferritin cage. Therefore, the RGD-4C peptide was incorporated at the N-terminus of the HFn subunit to present 24 copies of the targeting peptide. To accomplish this, an *Aat*II restriction site was introduced into the native HFn for subsequent incorporation of the RGD-4C peptide sequence. Primers were designed as follows to change a tyrosine (ACC) to a serine (TCC) at amino acid position 3 of HFn: (+) 5′ GAA GAA GAT ATA CAT ATG ACG TCC GCG TCC ACC TCG CAG GTG 3′; (−) 5′ CAC CTG CGA GGT GGA CGC GGA CGT CAT ATG TAT ATC TCC TTC 3′. To incorporate the RGD-4C peptide sequence onto the N-terminus of the HFn, the complimentary primers 5′ GC GAC TGC CGC GGA GAC TGC TTC TGC GGA GGC GGA ACG T 3′ and 5′ TCC GCC TCC GCA GAA GCA GTC TCC GCG GCA GTC GCA CGT 3′ were designed and inserted into the introduced *Aat*II site of the plasmid. Three glycine

(19) Flenniken, M. L.; Willits, D. A.; Brumfield, S.; Young, M.; Douglas, T. *Nano lett.* **2003**, *3*, 1573.
(20) Flenniken, M. L.; Liepold, L. O.; Crowley, B. E.; Willits, D. A.; Young, M. J.; Douglas, T. *Chem. Commun. (Cambridge)* **2005**, 447.
(21) Mann, S.; Meldrum, F. C. *Adv. Mater.* **1991**, *3* (6), 316.
(22) Mann, S.; Archibald, D. D.; Didymus, J. M.; Douglas, T.; Heywood, B. R.; Meldrum, F. C.; Reeves, N. J. *Science* **1993**, *261* (5126), 1286.
(23) Douglas, T.; Dickson, D. P. E.; Betteridge, S.; Charnock, J.; Garner, C. D.; Mann, S. *Science* **1995**, *269* (5220), 54.
(24) Wong, K. K. W.; Douglas, T.; Gider, S.; Awschalom, D. D.; Mann, S. *Chem. Mater.* **1998**, *10*, 279.
(25) Douglas, T.; Young, M. *Nature* **1998**, *393*, 152.
(26) Douglas, T.; Stark, V. T. *Inorg. Chem.* **2000**, *39*, 1828.
(27) Allen, M.; Willits, D.; Mosolf, J.; Young, M.; Douglas, T. *Adv. Mater.* **2002**, *14* (21), 1562.
(28) Allen, M.; Willits, D.; Young, M.; Douglas, T. *Inorg. Chem.* **2003**, *42*, 6300.
(29) Okuda, M.; Iwahori, K.; Yamashita, I.; Yoshimura, H. *Biotechnol. Bioeng.* **2003**, *84* (2), 187.
(30) Yamashita, I.; Hayashi, J.; Hara, M. *Chem. Lett.* **2004**, *33* (9), 1158.
(31) Ueno, T.; Suzuki, M.; Goto, T.; Matsumoto, T.; Nagayama, K.; Watanabe, Y. *Angew. Chem., Int. Ed.* **2004**, *43* (19), 2527.
(32) Kramer, R. M.; Li, C.; Carter, D. C.; Stone, M. O.; Naik, R. R. *J. Am. Chem. Soc.* **2004**, *126*, 13282.
(33) Varpness, Z.; Peters, J. W.; Young, M.; Douglas, T. *Nano Lett.* **2005**, *5*, 2306.
(34) Klem, M. T.; Willits, D.; Solis, D. J.; Belcher, A. M.; Young, M.; Douglas, T. *Adv. Funct. Mater.* **2005**, *15* (9), 1489.
(35) Tsukamoto, R.; Iwahor, K.; Muraoka, M.; Yamashita, I. *Bull. Chem. Soc. Jpn.* **2005**, *78* (11), 2075.
(36) Iwahori, K.; Yoshizawa, K.; Muraoka, M.; Yamashita, I. *Inorg. Chem.* **2005**, *44*, 6393.
(37) Okuda, M.; Kobayashi, Y.; Suzuki, K.; Sonoda, K.; Kondoh, T.; Wagawa, A.; Kondo, A.; Yoshimura, H. *Nano Lett.* **2005**, *5*, 991.
(38) Chasteen, N. D.; Harrison, P. M. *J. Struct. Biol.* **1999**, *126* (3), 182.
(39) Harrison, P. M.; Arosio, P. *Biochim. Biophys. Acta Bioenerg.* **1996**, *1275* (3), 161.
(40) Grossman, M. J.; Hinton, S. M.; Minakbernero, V.; Slaughter, C.; Stiefel, E. I. *Proc. Nalt. Acad. Sci. U.S.A.* **1992**, *89* (6), 2419.
(41) Lawson, D. M.; Artymiuk, P. J.; Yewdall, S. J.; Smith, J. M. A.; Livingstone, J. C.; Treffry, A.; Luzzago, A.; Levi, S.; Arosio, P.; Cesareni, G.; Thomas, C. D.; Shaw, W. V.; Harrison, P. M. *Nature* **1991**, *349* (6309), 541.
(42) Chatterji, A.; Ochoa, W.; Shamieh, L.; Salakian, S. P.; Wong, S. M.; Clinton, G.; Ghosh, P.; Lin, T. W.; Johnson, J. E. *Bioconjugate Chem.* **2004**, *15*, 807.
(43) Arap, W.; Pasqualini, R.; Ruoslahti, E. *Science* **1998**, *279* (5349), 377.
(44) Ruoslahti, E.; Duza, T.; Zhang, L. *Curr. Pharm. Des.* **2005**, *11* (28), 3655.
(45) Ruoslahti, E. *Nat. Rev. Cancer* **2002**, *2* (2), 83.
(46) Ruoslahti, E.; Rajotte, D. *Annu. Rev. Immunol.* **2000**, *18*, 813.
(47) Mulder, W. J. M.; Koole, R.; Brandwijk, R. J.; Storm, G.; Chin, P. T. K.; Strijkers, G. J.; Donega, C. D.; Nicolay, K.; Griffioen, A. W. *Nano Lett.* **2006**, *6*, 1.
(48) Kim, J. W.; Lee, H. S. *Int. J. Mol. Med.* **2004**, *14* (4), 529.

residues and one threonine residue were added after the RGD-4C peptide to allow for some structural flexibility. These mutagenesis experiments resulted in the change of the original HFn amino acid sequence MTTAS to MT*CDCRGDCFCGGGTS*AS. The RGD4C-Fn plasmid was isolated and sequenced as previously described for HFn.

Purification and Characterization of Ferritin. The HFn and RGD4C-Fn were expressed in *E. coli* where they self-assembled into the 24 subunit cages. Cultures of 1 L each of *E. coli* (BL21 (DE3): Novagen) containing pET-30a(+) HFn or RGD4C-Fn plasmid were grown overnight in LB medium with 30 mg/L kanamycin. RGD4C-Fn protein production was induced by IPTG (1 mM), and cells were incubated for an additional 4 h. After the incubation, cells were collected by centrifugation and then the pellets were resuspended in 45 mL of lysis buffer (100 mM HEPES, 50 mM NaCl, pH 8.0). Lysozyme, DNAse, and RNAse were added to final concentrations of 50, 60, and 100 μg/mL, respectively. After 30 min incubation at room temperature, the solution was subjected to French press followed by sonication on ice. The solution was centrifuged to remove *E. coli* debris. The supernatant was heated at 60 °C for 10 min, precipitating many of the *E. coli* proteins, which were removed by centrifugation. The supernatant was subjected to size exclusion chromatography (SEC; Amersham-Pharmacia, Piscataway, NJ) with a Superose 6 column to purify HFn or RGD4C-Fn. The protein cages were characterized using SEC, dynamic light scattering (DLS; Brookhaven, 90Plus particle size analyzer), and transmission electron microscopy (TEM; LEO 912AB). Protein concentration was determined by absorbance at 280 nm. Typically yields were 100 mg for HFn and 10 mg for RGD4C-Fn (isolated protein) per 1 L batch.

Iron Oxide Mineralization and Characterization. A degassed solution (8.0 mL of 100 mM NaCl) was added to a jacketed reaction vessel under an N_2 atmosphere followed by addition of HFn (2.0 mg, 3.9 nmol) or RGD4C-Fn (2.1 mg, 3.9 nmol) in 100 mM NaCl (either of HFn or RGD4C-Fn is 1.0 mg/mL) to the vessel. The temperature of the vessel was kept at 65 °C using circulating water through the jacketed flask. The pH was titrated to 8.5 using 50 mM NaOH (718 Auto Titrator, Brinkmann). Fe(II) was added (12.5 mM $(NH_4)_2Fe(SO_4)\cdot 6H_2O$) to attain a theoretical loading factor of 1000 Fe (313 μL), 3000 Fe (939 μL), or 5000 Fe (1566 μL) per protein cage. Stoichiometric equivalents (1:3 H_2O_2:Fe(II)) of freshly prepared degassed H_2O_2 (4.17 mM) was also added as an oxidant (reaction 1). The Fe(II) and H_2O_2 solutions were added simultaneously at a constant rate of 31.3 μL/min (100 Fe/(protein·min)) using a syringe pump (Kd Scientific). H^+ generated during the reaction was titrated dynamically using 50 mM NaOH to maintain a constant pH 8.5. The reaction was considered complete 5 min after addition of all the iron and oxidant solutions. After the completion of the reaction, 200 μL of 300 mM sodium citrate was added to chelate any free iron. Horse spleen apo ferritin (Sigma Chemicals Ltd., USA) was also subjected to the mineralization reaction with a theoretical loading factor of 1000 Fe/cage using the same procedure. The mineralized sample was analyzed using SEC with Superose 6. Absorbances at 280 and 410 nm were simultaneously monitored for protein and mineral, respectively. The sample was imaged by TEM, and electron diffraction and electron energy loss spectroscopy (EELS) data were collected on all samples.

$$3Fe^{2+} + H_2O_2 + 2H_2O \xrightarrow{65°C} Fe_3O_4 + 6H^+ \quad (1)$$

Magnetic characterizations of the mineralized samples were performed on a physical properties measurement system (PPMS; Quantum Design). Dynamic and static magnetic measurements were carried out using an alternating current magnetic susceptibility (ACMS) and a vibrating sample magnetometer (VSM) option, respectively. ACMS measurements were performed under a 10 Oe field at frequencies of 100, 500, 1000, 5000, and 10 000 Hz, with no direct current (dc) background, while the temperature was varied from 100 to 4 K. The superparamagnetic blocking temperature was determined from susceptibility curves. VSM measurements were performed under a magnetic field up to 80 kOe at 5 K.

C32 Amelanotic Melanoma Cell Culture. Human amelanotic melanoma cell line, C32, was purchased from the American Type Culture Collection (ATCC CRL-1585). C32 cells were cultured in Minimum Essential Medium Eagle (MEME, ATTC 30−2003) supplemented with 10% fetal bovine serum (Atlanta Biologicals, Norcross, GA), 100 units/(mL of penicillin) and 100 μg/(mL of streptomycin) at 37 °C in 5% CO_2 atomosphere.

Cell-Targeting Assay of Mineralized RGD4C-Fn. The mineralized RGD4C-Fn with a loading factor of 3000 Fe/cage was used to evaluate the ability of the protein cage to target cancer cells. The mineralized HFn cages (3000 Fe/cage) was used as a control. C32 cells were cultured in a six-well polystyrene plate. After 2 days of incubation, MEME was removed from the well followed by addition of 1 mL of mineralized protein (200 μg/mL) in Dulbecco's phosphate buffered saline (DPBS) and then incubated at 37 °C for 30 min. After the incubation, the solution was aspirated and washed 2 times with DPBS.

Cells were fixed in 3% glutalaldehyde in 0.1 M potassium sodium phosphate buffer (PSPB) at pH 7.2 for 10 min at room temperature. Following removal of gultalaldehyde, 1 mL of DPBS was added and cells were scraped using a rubber policeman and then centrifuged. Cell pellets were mixed with 50 μL of 4% agar solution and allowed to solidify. Agar pellets were then placed in 3% gultalaldehyde in PSPB overnight at 4 °C. Glutalaldehyde was removed and pellets were rinsed 2× with PSPB for 10 min each time. The pellets were then fixed for 4 h at room temperature followed by dehydrations steps of 50, 50, 70, 95, 100, 100, and 100% ethanol for 10 min each. Propylene oxide was used as a transitional solvent before infiltration with Spurr's embedding resin.[49] Cell pellets were thick and thin sectioned prior to imaging by TEM. The surface lengths of the cells were measured and the number of iron oxide clusters were counted on each image, to estimate the number of cluster per micrometer of cell surface.

Labeling of Ferritin with Activated Fluorescein Dye. Fluorescein-5-maleimide, which is capable of reactivity with cysteine residues present on proteins, was used for fluorescence labeling of ferritin. Either HFn or RGD4C-Fn in buffer (100 mM HEPES, 50 mM NaCl, pH6.5) was reacted with fluorescein-5-maleimide (Molecular Probes, Eugene, OR) in a concentration of 3 mol equiv per ferritin subunit at room temperature for 30 min followed by overnight incubation at 4 °C.[19,20] Fluorescein-labeled protein cages were purified from free dye using SEC as described above. The number of fluorescein linked per protein cage was determined using absorbance spectroscopy as previously described.[19]

Fluorescence-Activated Cell Sorting (FACS) Analysis of C32 Cells Incubated with Fluorescein-Conjugated RGD4C-Fn. Flow cytometry was performed on a FACSCalibur (Becton Dickinson, Mountain View, CA) and analyzed using Cell Quest software (Becton Dickinson). In order to perform the analysis, C32 cells were nonenzymatically removed from cell culture dishes by DPBS (without Ca^{2+} and Mg^{2+}) with 1% ethylenediaminetetraacetic acid (EDTA), washed once with serum containing MEME, and then suspended in DPBS (with Ca^{2+} and Mg^{2+}). The cells were incubated with fluorescently labeled protein cages (normalized to 2 μM fluorescein) in DPBS (with Ca^{2+} and Mg^{2+}) at a concentration of 2.5×10^6 cells/mL on ice for 20 min. After the incubation, the cells were washed 2 times with DPBS (with Ca^{2+} and Mg^{2+}) and then resuspended in DPBS (with Ca^{2+} and Mg^{2+}). To demonstrate selective binding of RGD4C-Fn to cancerous cells, a control experiment using non-cancerous T cells, which do not express $\alpha_v\beta_3$ integrins, were subjected to FACS analysis in the same manner as the C32 cell experiments described earlier. The binding specificity of RGD4C-Fn was also investigated in competition experiments, in which C32 cells were preincubated with increasing concentrations (55

(49) Spurr, A. R. *J. Ultrastruct. Res.* **1969**, *26* (1−2), 31.

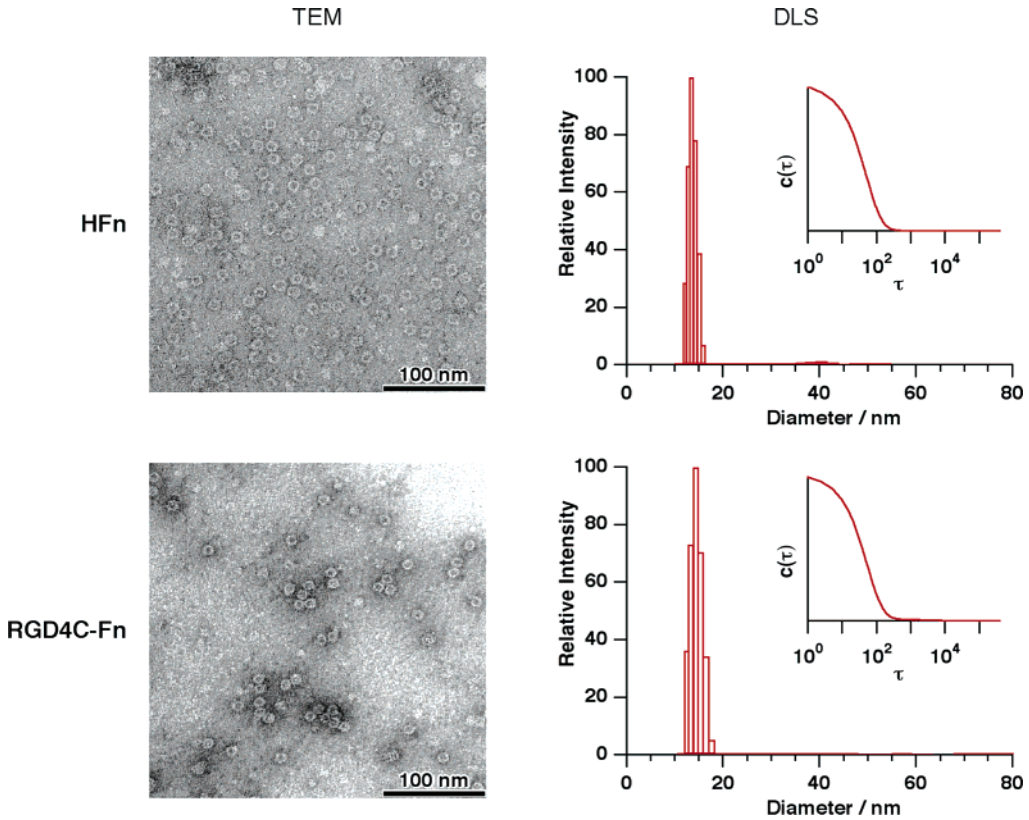

Figure 1. TEM images (left) and DLS analysis (right; insets are the corresponding correlation functions) of empty HFn and RGD4C-Fn. Both HFn and RGD4C-Fn show 12−14 nm in diameter.

μg/mL to 1.1 mg/mL) of either RGD4C-Fn or HFn (unlabeled) prior to incubation with fluorescently labeled RGD4C-Fn.

Results and Discussion

We have combined two important aspects of biological approaches to materials synthesis to form functional magnetic materials with the ability to target specific cells. Cell and tissue specific targeting peptides (RGD-4C), identified by in vivo phage display, have been genetically incorporated into the subunits of human H-ferritin (HFn), giving rise to a self-assembled cage architecture capable of both cell targeting and biomimetic mineralization. In this study, we present data on the ferrimagnetic iron oxide nanoparticle synthesis and characterization using both the HFn cage architectures and the cancer cell targeting variant of the HFn cage architecture, RGD4C-Fn. In addition, the efficacy of cell targeting is demonstrated on fluorescently labeled HFn and RGD4C-Fn using FACS analysis.

Both the HFn and RGD4C-Fn were heterologously expressed in *E. coli*. The purified proteins were analyzed by transmission electron microscopy, which revealed that both HFn and RGD4C-Fn adopted the expected spherical cagelike structures with a diameter of approximately 12 nm and that the two cages were indistinguishable (Figure 1). The self-assembled cages were further assessed using dynamic light scattering and found to be monodisperse in solution (Figure 1) with no significant difference in size between HFn (mean = 13.4 nm) and RGD4C-Fn (mean = 14.0 nm). Likewise, analysis of both HFn and RGD4C-Fn protein cage architectures by size exclusion chromatography exhibited identical elution times (data not shown). These results indicate that fusion of the RGD-4C peptide to the N-terminus of the HFn subunit does not interfere with the self-assembly of the subunits to form the characteristic 24 subunit protein cage architecture of ferritin.

The purified protein cages were subjected to synthetic iron oxide mineralization under conditions of elevated pH and temperature in order to direct the formation of the ferrimagnetic phase Fe_3O_4 (or γ-Fe_2O_3). Briefly outlined, solutions of Fe(II) and oxidant (H_2O_2) were added via syringe pump to the apoferritin cages under an atmosphere of N_2 at pH 8.5 and elevated temperature (65 °C) over a defined time period (10, 30, or 50 min). The reaction was performed using a range of stoichiometric "loading factors" ranging from 1000 to 5000 Fe/cage. In the presence of the HFn, or RGD4C-Fn, a homogeneous brown colored solution was obtained after the reaction for all loading factors. Control reactions, run in the absence of the protein cages, resulted in bulk precipitation of the iron oxide from solution. Unstained products of protein-mediated mineralization were observed by TEM and showed electron-dense nanoparticles (Figure 2). The average diameter of the particles increased from 3.8 to 6.0 nm as the loading factor was increased from 1000 to 5000 Fe/cage. There was no significant difference in particle size between the products mediated by the HFn and RGD4C-Fn. This indicates that RGD-4C peptide, on the exterior surface of the cage, had little effect on the mineralization process, even though there are four cysteine residues present in the peptide. Electron energy loss spectroscopy of the particles showed the iron L_{23} spectrum (Figure 3) and selected area electron diffraction from a collection of particles in both the mineralized RGD4C-Fn and HFn exhibited powder diffraction patterns, which could be ascribed to either maghemite or magnetite (Figure 3 and Table 1).

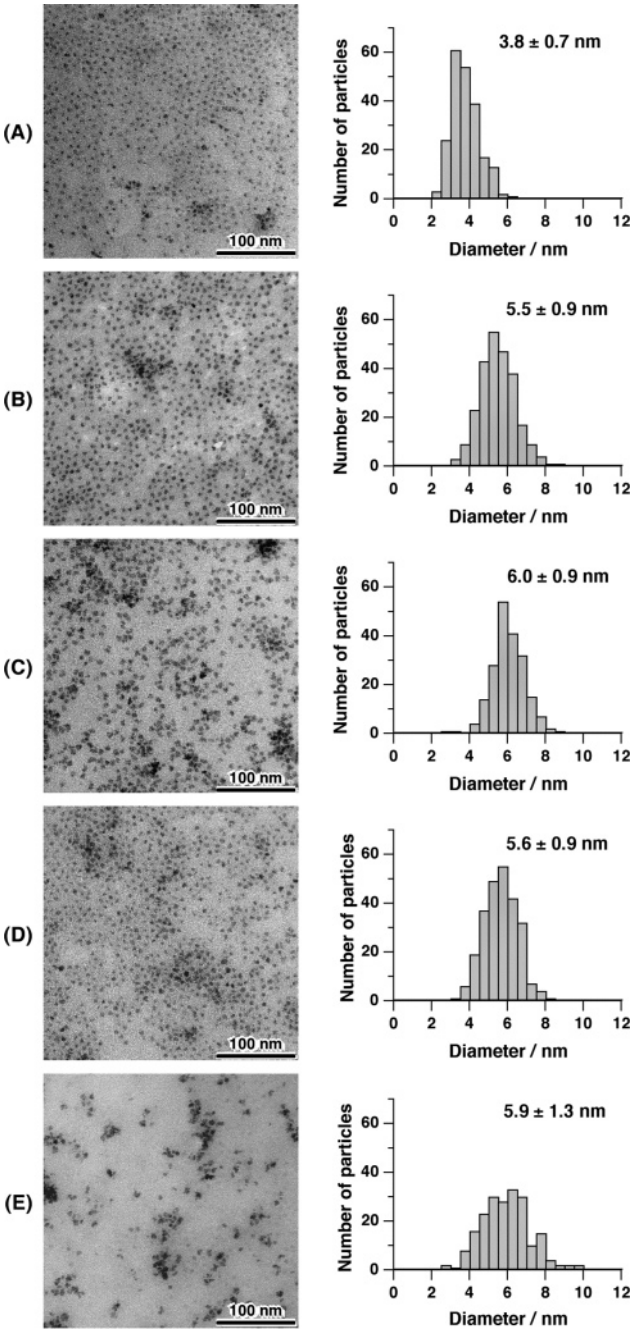

Figure 2. TEM images and size distribution histograms as measured by TEM of mineralized RGD4C-Fn, HFn, and HoSpFn under various loading factors of Fe. The values shown on the histograms are mean ± standard deviation: (A) RGD4C-Fn 1000 Fe/cage; (B) RGD4C-Fn 3000 Fe/cage; (C) RGD4C-Fn 5000 Fe/cage; (D) HFn 3000 Fe/cage; (E) HoSpFn 1000 Fe/cage. The size of the particles formed inside of RGD4C-Fn increase with increasing loading factor of Fe per cage. There is no significant difference in size between particles formed inside of HFn and RGD4C-Fn under the same loading factor. Particles formed within HoSpFn are larger in size and wider distribution than those formed within RGD4C-Fn.

It should be noted that the size (volumes) of the Fe_3O_4 cores formed inside of the HFn and RGD4C-Fn are smaller than those formed inside horse spleen ferritin (both prepared in this experiment and in a previous report[24]) and closer to the theoretical core diameters calculated for a uniform spherical particle of the cubic iron oxide (either Fe_3O_4 or γ-Fe_2O_3) phase at these loading stoichiometries (Figure 2 and Table 2). This suggests that the HFn and the RGD4C-Fn mutant are superior

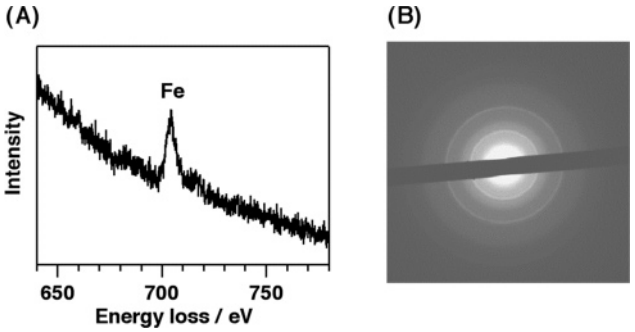

Figure 3. (A) EELS of mineralized RGD4C-Fn with loading factor of 3000 Fe/cage. (B) Selected area electron diffraction pattern of mineralized RGD4C-Fn with loading factor of 3000 Fe/cage.

Table 1. *d*-Spacing for Maghemite and Magnetite and Measured *d*-Spacing for Mineralized RGD4C-Fn with a Loading Factor of 3000 Fe/Cage

d-spacing of maghemite	*d*-spacing of magnetite	measd *d*-spacing
2.518	2.532	2.54
1.476	1.485	1.49

Table 2. Comparison of Measured Iron Core Diameter in RGD4C-Fn, Previously Reported Iron Core Diameter in Horse Spleen Fn, and Calculated Theoretical Diameter

theor iron loading, atoms/(protein cage)	mean iron core diam in RGD4C-Fn, nm	mean iron core diam in horse spleen Fn, nm	calcd theor iron core diam, nm
260		5.7[b]	2.3
1000	3.8[a]	5.9,[a] 7.5[b]	3.6
3000	5.5[a]	8.4[b]	5.2
5000	6.0[a]		6.2

[a] The data were obtained in this experiment. [b] The data were from ref 24.

platforms for the homogeneous nucleation of iron oxide inside of the protein cage as compared to horse spleen apo-ferritin. This interesting difference is probably due to the difference of subunit composition between HFn and horse spleen ferritin. Native mammalian ferritins consist of mixtures of two different subunit types: H (heavy) and L (light) chain. Horse spleen ferritin is a mixture of about 15% H chain and 85% L chain subunits, while HFn is a homopolymer of only H chain.[39] The H chain contains a catalytic ferroxidase site (absent in L chain), which is responsible for Fe(II) oxidation to Fe(III).[41] In ferritin, oxidation of Fe(II) is followed by spontaneous nucleation due to extremely low Fe(III) solubility. The enhanced control over particle size exhibited by our results with HFn suggests that the ferroxidase site plays an important role in iron oxide nucleation even under these fairly harsh synthetic conditions. It further suggests also that under these (nonphysiological) conditions the ferroxidase site in HFn is able to utilize H_2O_2, a function previously only ascribed to related bacterioferritins.

For both the HFn and RGD4C-Fn the mineralization occurred in a spatially selective manner and the reaction did not disrupt the protein cage in any measurable way. SEC analysis of the RGD4C-Fn before and after mineralization with 3000 Fe/cage (Figure 4) showed coelution of the protein cage (280 nm) and the mineral core (410 nm), whereas before the mineralization, protein shows no absorption at 410 nm. In addition, the retention time of the mineralized protein cage was identical to the cage before mineralization. This elution behavior indicates the protein−mineral composite nature of the material and suggests that the overall structure of the protein cage has not been

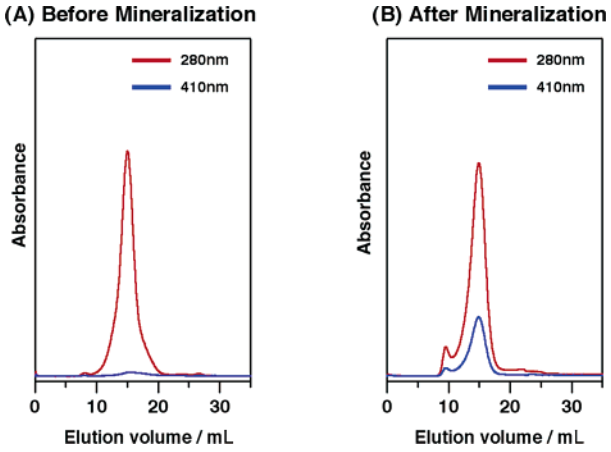

Figure 4. SEC of RGD4C-Fn (A) before mineralization reaction and (B) after mineralization with 3000 Fe/cage. Elution was monitored at both 280 nm (protein) and 410 nm (iron oxide mineral). Coelution of protein and mineral in profile B indicate the composite nature of the mineralized protein cage.

significantly perturbed by the mineralization process. The iron oxide mineral is clearly encapsulated and sequestered within the protein cage as a result of the mineralization reaction.

Magnetic characterization using a physical properties measurement system (PPMS) was used to probe the size-dependent magnetic properties of the mineralized cages. Using alternating current magnetic susceptibility (ACMS), the blocking temperature (T_b) of the samples was found to increase with increasing particle size from 11 K for the 1000 Fe loading to 27 K for the 3000 Fe loading to 36 K for Fe loading factor of 5000 ions, as shown in Figure 5. Data was analyzed using the Neel−Arrhenius equation

$$\ln(1/f) = \ln(1/\Gamma_0) + \frac{E_a}{k_B}\frac{1}{T_b} \qquad (2)$$

where f is the measurement frequency, Γ_0 is the attempt frequency, E_a is the anisotropy energy, and T_b is the blocking temperature. By measuring the susceptibility of a sample at multiple frequencies, a fit to the Neel−Arrhenius equation was obtained. As shown in Figure 6, Neel−Arrhenius fits showed linear behavior for all three samples. Since eq 2 is the expected behavior of an isolated particle, the linear behavior indicates that the particles are encapsulated within the protein cages and clearly not interacting with each other. Vibrating sample magnetometry (VSM) measurements revealed that all samples exhibited superparamagnetic behavior at room temperature since no hysteresis was observed at 300 K. At 5 K, ferrimagnetic components were evident in the magnetic behaviors of all samples (Figure. 7). Coercive fields (Hc) of 720, 550, and 620 G was observed for 1000, 3000, and 5000 Fe/cage, respectively. These results indicate that magnetic properties of the mineralized ferritin can be adjusted accordingly by controlling synthesis conditions, in particular the Fe to protein stoichiometry.

To test the targeting efficacy of the RGD4C-Fn construct, we compared its binding to C32 amelanotic melanoma cells. C32 cells overexpress the $\alpha_v\beta_3$integrins on their cell surface, and these are known to be the recognition sites for the RGD-4C (CDCRGDCFC) peptide.[43] Cells were incubated with either the RGD4C-Fn or HFn and subsequently washed, thin-sectioned, and imaged by TEM. As shown in Figure 8, clusters of small

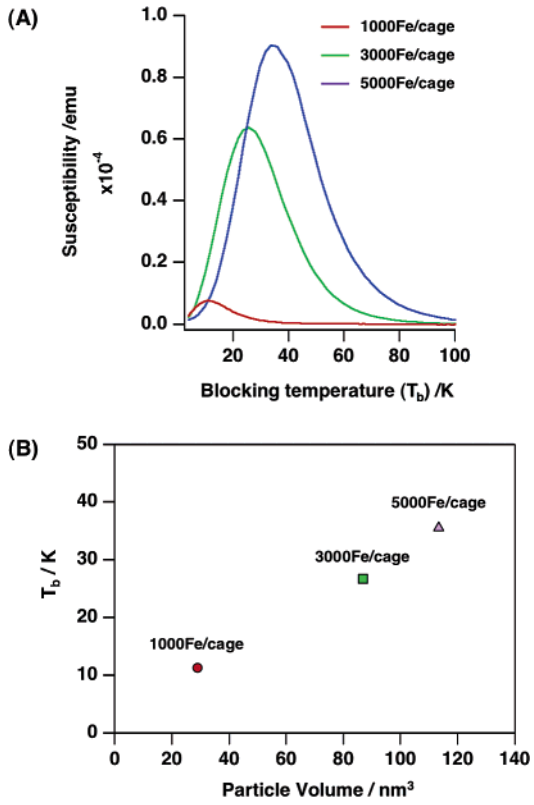

Figure 5. (A) ACMS measurement of mineralized RGD4C-Fn with various loading factors under 10 Oe field at 1000 Hz. (B) Plot of blocking temperature (T_b) at 1000 Hz against particle volume for mineralized core.

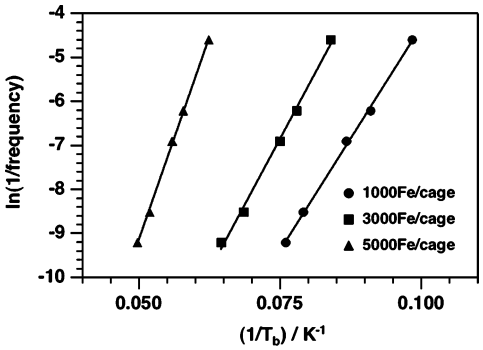

Figure 6. Neel−Arrhenius fits showing the frequency dependence of the blocking temperature of each sample, according to eq 2. Here, the inverse blocking temperatures of the 3000 and 5000 Fe/cage samples have been scaled by 2 to more clearly display the linearity of the data. The linear behavior of each data set indicates that the particles are noninteracting.

electron-dense particles were easily found on the surface of the cells, corresponding to the mineral core within the ferritin cages. These clusters were absent in cells not incubated with mineralized RGD4C-Fn or HFn. While some clusters were observed in cells incubated with HFn, their number density was significantly lower than for cells incubated with RGD4C-Fn cages (roughly 50% lower). This indicates that the RGD-4C peptide moiety affords enhanced targeting capacity to the mineralized Fn cage.

To quantitate the cancer cell binding ability of the RGD4C-Fn, fluorescence activated cell sorting (FACS) analysis was performed using fluorescein-labeled cages (RGD4C-Fn and HFn). The number of fluorescein molecules conjugated to the protein cages was determined by absorbance spectroscopy to be 0.6/subunit (14.4/cage) for HFn and 0.8/subunit (19.2/cage)

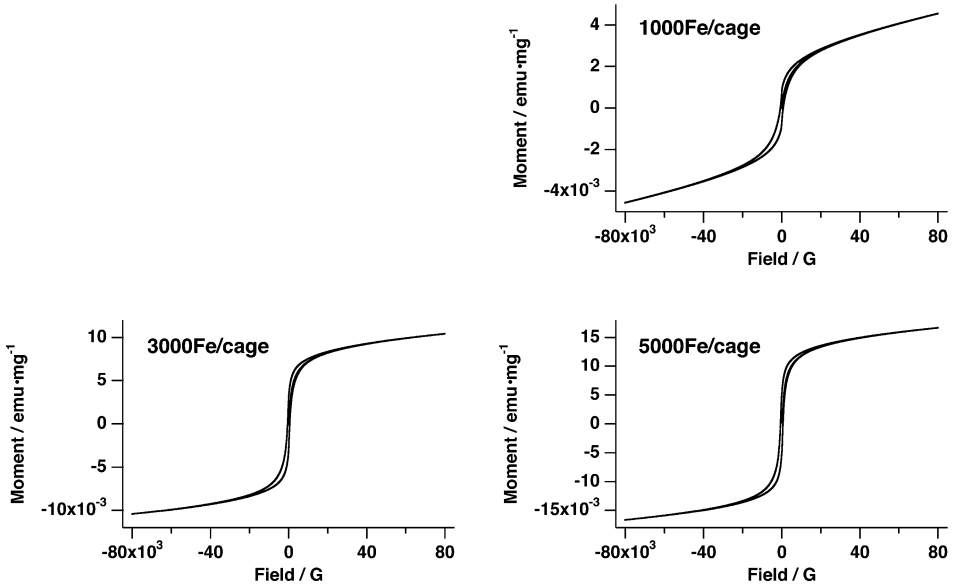

Figure 7. Hysteresis loops (magnetization versus applied field) at 5 K for mineralized RGD4C-Fn.

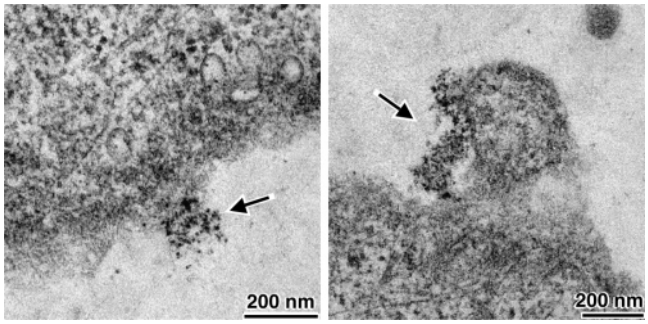

Figure 8. TEM micrographs of C32 cell incubated with mineralized RGD4C-Fn with loading factor of 3000 Fe/cage for 30 min. Arrows indicate mineralized ferritin.

for RGD4C-Fn (data are not shown), whereas the number of exterior surface exposed cysteine residues was 2 and 6, respectively. These data suggest that the four additional cysteines of the RGD4C peptide do not participate in the conjugation reaction.

The result of FACS analysis indicates that RGD4C-Fn exhibits enhanced C32 melanoma cell targeting ability (Figure 9). C32 cells incubated with fluorescein-labeled RGD4C-Fn had a geometric (geo.) mean fluorescence intensity value of 1972, whereas the cells exhibit autofluorescence with geo. mean fluorescence intensity value of 36. Although the C32 cells incubated with nontargeted ferritin cage (HFn) did exhibit some nonspecific interaction (geo. mean fluorescence intensity value of 568), this is significantly smaller than for cells incubated with RGD4C-Fn. These data are consistent with those obtained from TEM observation of C32 cells incubated with the ferritin cages.

To demonstrate the specificity for the $\alpha_V\beta_3$ intergtrins, control (non-cancerous) T cells were analyzed for their ability to bind RGD4C-Fn. Cells were incubated with either RGD4C-Fn or HFn, and both exhibited a similar background level of nonspecific binding, several orders of magnitude below the binding observed in C32 experiments. Geo. mean fluorescence intensity values of these two cases (15 and 25, respectively) were close to that of the T cells without incubation of any fluorescently labeled protein cage (Supporting information Figure S1). This

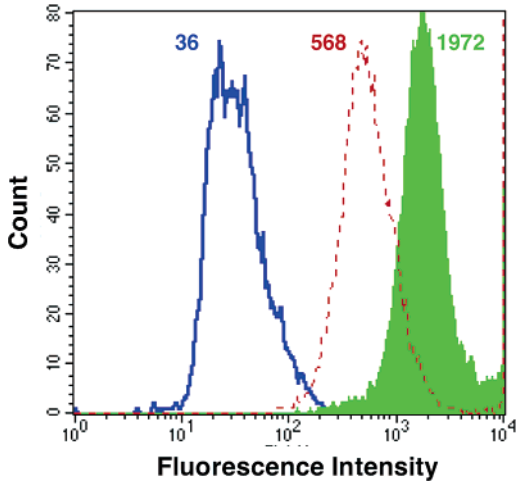

Figure 9. FACS analysis of C32 melanoma cells incubated with fluorescence-labeled protein cages. The data are plotted as histograms with their corresponding geometric (geo.) mean fluorescence values. The blue solid line indicates cells not incubated with RGD4C-Fn or HFn (geo. mean = 36). The red dashed line indicates cells incubated with fluorescein-labeled HFn (geo. mean = 568). The green filled plot indicates cells incubated with fluorescein-labeled RGD4C-Fn (geo. mean = 1972). The increased level of fluorescence intensity of the cells incubated with fluorescein-labeled RGD4C-Fn indicates specific binding of the cages to C32 melanoma cells.

result clearly indicates that RGD4C-Fn cages lack specific binding ability to non-cancerous T cell. In addition, competition experiments were performed to evaluate the specificity of binding. C32 cells were preincubated with increasing amounts (55 μg/mL to 1.1 mg/mL) of either RGD4C-Fn or HFn (unlabeled) prior to incubation with fluorescently labeled RGD4C-Fn. FACS analysis revealed that unlabeled RGD4C-Fn could effectively compete for binding with the labeled RGD4C-Fn, wheras HFn was far less effective in competitive binding (Supporting information Figure S2). Together these results indicate that RGD4C-Fn exhibits specific targeting capacity toward cancerous cells expressing high levels of $\alpha_v\beta_3$ integrins. These results hold the promise for successful targeting to angiogenic tumor vasclutature.

The result of C32 cell specific binding of RGD-4C conjugated ferritin is similar to a previous report in which the ability of

small heat shock protein genetically modified to incorporate the RGD-4C peptide to bind cancer cells was investigated.[3] This illustrates the versatility of our approach, which has wide applicability for a variety of protein cages. A library of protein cage architectures having a range of sizes is available and thus extends the utility of this approach for size-dependent cage-property selection. Furthermore, it is expected that genetic incorporation of cell binding peptide onto the exterior surface of protein cages has the potential for applications in cell specific therapeutic and imaging delivery system because not only the RGD-4C peptide but also many other cell-targeting peptides could be incorporated into protein cage architectures using essentially the same approach.

Conclusion

We have demonstrated that the human H-chain ferritin cage can serve as a multifunctional platform for the biomimetic synthesis of magnetic nanoparticles and can be engineered for use as a cell-specific targeting moiety. The present work reveals two important points. First, both HFn and RGD4C-Fn can be used as a constrained reaction environment for the synthesis of superparamagnetic magnetite and/or maghemite without perturbing its cage-like architecture. This means that the exterior surfaces of protein cage architectures can be modified without altering the function of the cage as a size-constrained reaction vessel. Second, the mineralized RGD4C-Fn exhibits increased specific targeting interaction with a cancer cell as compared to the control HFn. The magnetic and cell targeting capabilities engineered into this protein cage makes it ideal as a new diagnostic imaging agent. This demonstrates the ability to add multifunctionality such as cell targeting, imaging, and perhaps therapeutic agents simultaneously to a single protein cage. The utility of these materials for in vivo targeted diagnostic imaging are currently being evaluated. This work extends the diverse applications of protein cages in the field of biomedicine because the current approach is applicable in modifying other protein cages or introducing other cell-targeting peptides to a protein cage.

Acknowledgment. This research was supported in part by grants from the National Institutes of Health (Grant R21EB005364) and the Office of Naval Research (Grants 19-00-R006 and N00014-03-1-0692). M.U. was supported by a Grant-in-Aid for Scientific Research for Young Scientists from the Ministry of Education, Culture, Sports and Technology, Japan. M.L.F. was supported by a Ruth L. Kirschtein fellowship from NIH (Grant F31 EB005093).

Supporting Information Available: FACS analysis, demonstrating the lack of binding to non-cancerous cells, using non-cancerous T cells, as described for the FACS analysis of C32 binding, and the binding specificity of RGD4C-Fn to C32 melanoma cells, investigated by competition experiment, in which C32 cells were preincubated with either RGD4C-Fn or HFn (not labeled with fluorescein) prior to incubation with fluorescently labeled RGD4C-Fn. These data are available free of charge via the Internet at http://pubs.acs.org.

JA0655690